Crustal block kinematics and seismic potential of the northernmost Philippine Sea plate and Izu microplate, central Japan, inferred from GPS and leveling data

Takuya Nishimura[1] , Takeshi Sagiya[2] and Ross S. Stein[3]

Geographical Survey Institute, Tsukuba, Ibaraki, Japan[1]
(Corresponding Author: t_nisimura@gsi.go.jp)
Nagoya University, Nagoya, Aichi, Japan[2]
U.S. Geological Survey, Menlo Park, California, USA[3]

31 May 2007

Abstract

We clarify the contemporary deformation observed by GPS and leveling for the greater Tokyo (Kanto, eastern Tokai, and the Izu islands) region, where the Izu-Ogasawara (Bonin) arc is subducting and colliding with the central part of the Japan arc. From these data, we develop a kinematic model of fault sources with variable components of seismic and aseismic slip. Under the assumption that the contemporary deformation during 1995-2000 is representative of the longterm interseismic strain field, the geodetic data are inverted to estimate the rotation poles of the crustal blocks, the degree of elastic strain accumulation on faults, and the volumetric inflation sources beneath volcanoes. The present crustal movements are explained by four crustal blocks: the Izu micro-plate, the Central Japan block, the Pacific plate, and the Philippine Sea plate. Along the Suruga and Sagami margins of the Philippine Sea plate lie strongly coupled faults, which include sites of the 1854 M=8.4 Tokai, 1923 M=7.9 Kanto, and 1703 M~8.2 Genroku Kanto earthquakes. In contrast, the Philippine Sea plate boundary immediately north of the Izu peninsula, site of M≤7.5 collisional earthquakes, is only weakly coupled. The boundary between the Izu micro-plate and the Philippine Sea plate experiences left-lateral motion with the rate of ~30 mm/yr. Most of this boundary is locked and thus has a large potential of future earthquakes. The Izu micro-plate is found to rotate rapidly clockwise at 10°/Myr, with a rotation pole relative to the Central Japan block located just north of its northern boundary. The pole and angular velocity of the Izu micro-plate depends, however, on the assumed location of the boundary. With the exception of the site of the 1938 M≥7 earthquake swarm, which we infer has the current potential to produce a M~8.1 earthquake, the Pacific megathrust has a very low seismic potential, although the geodetic data have little resolving power for much of the Pacific plate interface east of Tokyo.

1. Introduction

Central Japan is subjected to the collision of three, and arguably four, tectonic plates (Figure 1). The Philippine Sea and the Pacific plates are subducting beneath the Kanto region, central Japan. Carried north by the Philippine Sea plate, the Izu-Ogasawara (Bonin) arc is colliding with the southwestern part of the Kanto region at the Izu peninsula. The arc carries a chain of active volcanoes, including Miyakejima, which produced the A.D. 2000 seismic super-swarm and eruption [Nishimura et al, 2001; Toda et al, 2002], and Mt. Fuji, which last erupted in 1707. Historically, many damaging earthquakes have struck the Kanto and surrounding regions (Figure 2). The largest of these have occurred on the subduction plate boundary of the Philippine Sea plate along the Sagami and Suruga troughs. The M=7.9 1923 Kanto earthquake, which caused about 105,000 fatalities, occurred along the Sagami trough [Kanamori, 1971; Ando, 1971; Matsu'ura et al., 1980; Wald and Sommervile, 1995; Nyst et al., 2006]. The M~8.2 1703 Genroku Kanto earthquake ruptured both the source area of the 1923 earthquake and also its southeast extension [e.g. Ishibashi, 1977, Matsuda et al., 1978, Shishikura, 2003]. The M~8.4 1854 Ansei Tokai earthquake ruptured west of the Izu peninsula along the Suruga trough [e.g. Ando, 1975; Ishibashi, 1981]. In addition, shallow M~7 earthquakes often occur around the Izu peninsula. Understanding the present-day kinematics of Central Japan is important to assess the potential seismic and volcanic hazards faced by the economic and political center of this region.

Several previous studies interpreted the contemporary deformation in the Kanto and Tokai regions. Yoshioka et al. (1993, 1994) estimated the distribution of seismic coupling from geodetic data on the subducting plate boundaries along the Sagami and the Suruga troughs, respectively. They used trilateration and leveling data acquired from 1972 to 1990. Sagiya (1999, 2004) revisited the same regions using GPS data spanning the late 1990's. These studies regarded the deformation data on the overriding plates as the elastic deformation due to fault locking on the plate boundary, and estimated the spatial distribution of the degree of seismic coupling on the boundary. Here, 'coupling' refers to whether the subduction interface is frictionally locked and thus accumulating elastic strain, or is freely slipping (which is referred to as 'uncoupled').

We argue that a key to understanding the complex regional kinematics of the triple junction is the movement of the Izu peninsula, which is sometimes recognized as a microplate [e.g. Hashimoto and Jackson, 1993; Sagiya, 1999]. Mazzotti et al. (1999) first estimated the rigid rotation of the Izu micro-plate, which includes the Izu peninsula, from geomorphology, earthquake P-axes, and GPS data, but they did not study its elastic deformation. Henry et al. (2001) used elastic strain data on the overriding plate deduced from GPS data to estimate the motion of the downgoing Philippine Sea plate slab along the Suruga trough, and so estimated the rigid rotation of the

subducting Izu micro-plate.   Though these previous studies clarified part of the regional kinematics, the modeling of both the rigid rotation and elastic deformation has not been uniformly applied to the many complex regions, including the volcanic islands and collision zone north of the Izu peninsula, which we attempt here.

Unlike previous studies, newly available GEONET GPS data and additional leveling surveys permit us to estimate the rigid rotation and elastic deformation simultaneously. This enables us to constrain the kinematics with more fidelity than the previous analyses. After eliminating the effects of seismo-volcanic events and human activity from the observed data here we estimate the contemporary tectonic deformation field. We then develop a kinematic block-fault model, for which the surface velocity is the sum of the rigid rotation and the elastic deformation due to fault locking and volcanic sources.

2. Data and Analysis

2.1 GPS Data

We use continuous GPS data to estimate site velocity in the Kanto, the eastern Tokai, and the Izu regions, as shown in Figure 3.   We also estimate GPS site velocities on the Ogasawara and the Daito islands (Figure 1a) to constrain the motion of the Philippine Sea plate far from its boundaries. The continuous GPS observations in these regions were started as COSMOS-G2 by the Geographical Survey Institute (GSI) in 1994.   In April 1996, the GPS network was merged with the nationwide GPS network to become GEONET [Sagiya et al., 2000].   The GEONET data [Geodetic Observation Center, 2004] were recently re-analyzed using Bernese 4.2 software [Rothacher and Mervart, 1996], with daily coordinates in the International Terrestrial Reference Frame 2000 (ITRF 2000)[Altamimi et al., 2002].   We used these daily GEONET coordinates to estimate site velocities by fitting a linear trend and annual and semiannual sinusoidal curves according to

$$x(t) = a + bt + c\sin(2\pi t) + d\cos(2\pi t) + e\sin(\pi t) + f\cos(\pi t) + \sum_{n=1}^{m} g_n H(t - t_n) \qquad (1)$$

where $x(t)$ is one component of a GPS site, t is time, a, b, c, d, e, f, and g_n are unknown parameters, $H(t)$ is a step function representing an offset caused by a seismo-volcanic event or a GPS antenna replacement, t_n is the date when the nth event occurred, m is number of events. Examples of fitting (1) to the time series are shown in Figure 4.

Ideally, one would use as long a period as possible to estimate the secular velocity, but network augmentations and tectonic events must be accounted for.   The start date for the velocity estimation is when the GPS network was reorganized in April 1996.   Because new GPS stations

were added in April 1997 and April 1998, these dates are the start date for the new stations. We also include the GPS velocity of the Zenisu reef, 80 km south of the Izu peninsula (Figure 1b and 5), based on campaign GPS measurements on the isolated reef from August 1995 to August 1998 [Tabei et al., 1999]. A voluminous earthquake swarm started in June 2000 in the northern Izu islands (Figure 2), causing significant displacement over the Kanto and the Izu regions [Nishimura et al., 2001; Toda et al, 2002] that must be removed to estimate the secular strain field. Transient deformation following the swarm, as well as the slow slip event that occurred in the Tokai region during 2000-2005 [Ozawa et al., 2002], also complicate the estimation of the secular velocity in Tokai. Therefore, we have chosen to end the time series in May 2000, yielding a 4.17-year-long period.

Several seismo-volcanic events caused significant displacements at GPS stations near Ito, off the eastern Izu peninsula, from April 1996 to May 2000, with major events in March 1997, and April-May 1998 [Aoki et al., 1999; Nishimura, 2002]. To remove these displacements, we assumed that 5 March 1997 and 1 May 1998 were the event date (t_n) for the last term of Equation (1). Because two minor events occurred in 1996 (Figure 4b), we did not use the data of 13 stations near Ito from April to October 1996. Finally, a slow slip event also occurred off the Boso peninsula in May 1996 [Ozawa et al., 2003, Sagiya, 2004], with a peak GEONET displacement of 15 mm (Figure 4a). Because the slow slip event occurred early in the study period, its effect on the secular velocity is negligible, and so is ignored.

We converted the GPS velocities to the EUR (Eurasia Plate)-fixed frame by subtracting the motion of EUR from ITRF 2000, as calculated from the EUR-ITRF2000 Euler pole [Altamimi et al., 2002]. We chose the EUR-fixed reference frame because EUR motion is well resolved, and the motion of the Philippine Sea plate is often described by an Euler pole relative to the EUR. Studies of GPS time-series [e.g. Mao et al., 1999] show that errors in the GPS velocities may be underestimated by a factor of 2-11 if pure white noise is assumed, due to time-correlated noise, including flicker and random-walk. Dixon et al. (2000) proposed that the magnitude of the white and the flicker noises are correlated with the WRMS (weighted root mean square) scatter. We calculated the magnitude of the white and flicker noises following Dixon et al. (2000) and then estimated the total velocity uncertainties with Equation (20) from Mao et al. (1999). We neglect the random-walk noise component, which is not significant for our observation period. The resulting uncertainties of the GPS velocity range from 0.10 to 1.96 mm/yr for horizontal components, and from 1.30 to 6.51 mm/yr for vertical components.

The secular velocities in the Kanto region and its vicinity are characterized by westward movement in the EUR reference frame (Figure 5), suggesting that the Kanto and the eastern Tokai

regions do not belong to the Eurasian plate [Sagiya, 1999]. The vectors on the Izu islands show northwestward movement of the Philippine Sea plate and complex deformation patterns due to volcanism. The interpolated vertical velocities (Figure 5) show subsidence on the southern coast in the Kanto and Tokai regions. The subsidence around Omaezaki and the southern tip of the Boso peninsula suggests interplate coupling on the subduction megathrusts. In contrast, we attribute the rapidly subsiding areas north of Tokyo and in the eastern part of the Boso peninsula as the product of ground water pumping and natural gas extraction, respectively [Geographical Survey Institute, 1999]. A few horizontal vectors are not concordant with the surrounding vectors, probably resulting from landslides and monument instabilities. From a strain rate analysis of the GEONET in these regions, Itani and Ishibashi (2003) identified anomalous GPS stations. In our inversion analysis, we exclude stations found by Itani and Ishibashi, as well as two stations in the subsidence area in the eastern Boso peninsula. Two GPS stations in the subsidence area north of Tokyo are used in the inversion but are down-weighted by a factor of three. Some 176 GPS stations are used in the inversion.

2.2 Leveling data

Leveling surveys have been conducted every few years to monitor crustal deformation by tectonic and volcanic sources as well as land subsidence due to human activities. We use first-order leveling data carried out by GSI and the Chiba prefecture government. The Japanese first-order leveling is double-run with a tolerance limit of the difference between the forward and the backward measurements per section of $2.5\sqrt{L}$ in millimeters, where L is the length of the section in kilometers. The observation error s of leveling is given by $s = \alpha\sqrt{L}$, where s is in millimeters, α is the standard deviation calculated from several double-run sections. We adopt 0.49 mm/$\sqrt{\text{km}}$ for α, which is the average for all first-order leveling in Japan from 1985 to 1996 [Ohtaki, unpublished material].

Some 605 sections or 700 km of leveling <u>were</u> included in the analysis after careful screening for non-tectonic disturbances. We included routes that were leveled at least twice between 1995 and 2000. The vertical velocity for each section was calculated by dividing differences between two measurements by their inter-survey time, which ranges between 2.33 and 5.12 years. Because two measurements are independent, the uncertainties σ of the velocity data is given by $\sigma = 0.49 \cdot \sqrt{2} \cdot \sqrt{L}/t$, where σ in millimeters/year and t is inter-survey time in year. The leveling route is divided into 15 sub-routes (Figure 2), most of which follow Tokyo and Suruga bays, and the Miura and Izu peninsulas, and the Oshima and Miyakejima island coastlines. We did not use other leveling routes in the Izu peninsula and the eastern part of the Boso peninsula because the data

are heavily affected by the seismo-volcanic events and ground water pumping described previously and evident in the GPS vertical velocities (Figure 5). The first-order leveling benchmarks are arranged roughly every two kilometers along principal highways. The section distance between adjacent benchmarks, however, varied from a few meters to a few kilometers because of secondary benchmarks for road construction. In addition, the raw data show large subsidence troughs, indicative of local human activity and benchmark instability. To create a more homogeneous dataset for the inversion, we omitted leveling sections less than 500 m, and removed sections showing local disturbances by visual inspection. Subsidence was retained at km 50 and 100 of route 3, and at km 25 of route 4, although it is suspect because they locate in dense populated and industrial areas with no significant active faults,. This left 605 sections (Figure 6). The leveling routes extending to the tip of cape Omaezaki, Miura, and Boso Peninsula show downward flexure (Figures 6a, 6e, and 6l), which is consistent with the GPS velocities (Figure 5). Routes 14 and 15 show rapid deformation on Oshima and Miyakejima which are active volcanic islands.

3. Block-Fault Model

In the kinematic block-fault model, surface displacement are expressed by the sum of rigid block rotations and elastic deformation near faults [e.g. Matsu'ura et al., 1986, Hashimoto and Jackson, 1993; Meade et al., 2002; McCaffrey 2002; Wallace et al., 2004]. Rigid block rotation on a spherical Earth is formularized as follows,

$$\mathbf{v} = \omega \times \mathbf{r} \qquad (2)$$

where $\mathbf{v}$ is a velocity at a point $\mathbf{r}$ in a Cartesian coordinate system whose origin is the center of the Earth, and ω is an Euler vector of the rigid rotation. Because the rigid rotation causes only horizontal motion, vertical GPS and leveling data are essential to discriminate between block rotation and elastic deformation. The elastic deformation is caused by strain associated with locked faults that bound the tectonic blocks. The locking effect on the faults can be represented by a dislocation opposite to the relative movement of two adjacent blocks [Savage and Burford, 1973], or it can be considered 'back-slip' in the case of modeling of subducting plate boundary [Savage, 1983]. This nominal dislocation is often referred as a 'slip deficit,' presumably to be paid back in some forthcoming slip event such as an earthquake. We approximate block boundaries by rectangular faults whose geometry is fixed in the inversion. The relative motion on a block boundary is calculated from the Euler vectors of two crustal blocks. The slip(-deficit) rate is the only free parameter for each fault in the inversion because the rake angle of the slip is assumed to be dependent on the Euler vectors of the tectonic blocks. We calculate the relative motion between two blocks at the surface point directly above the center of each rectangular fault. The

7

rake of slip that accommodates relative block motion on the faults should be the angle between the fault strike and the direction of the horizontal movements. We assigned the rake of the slip-deficit as opposite to the rake of slip calculated in this way. Many previous studies of the block-fault models [e.g. Matsu'ura et al., 1986; Hashimoto and Jackson, 1993; Meade et al., 2002] estimate two independent components of the slip(-deficit), that is, strike-slip and dip-slip rates. Our approach thus reduces the number of free parameters with a reasonable assumption that the fault rake optimally accommodates the fault motion.

Elastic deformation due to dislocation sources is calculated following Okada (1985) assuming an elastic half-space. The sphericity of the medium can be neglected to calculate the elastic deformation, because an elastic half-space gives insignificantly different displacement from that of the spherical Earth within 100 km of a dislocation source [Pollitz, 1996]. In addition to the strain accumulation by the boundary faults, we used point inflation sources [Mogi, 1958] to represent deformation associated with the several active volcanoes in the Kanto and Izu regions (Figure 1b).

We simultaneously estimated the following parameters: the slip(-deficit) rate of the boundary faults, the location and inflation rate of point sources, and the Euler vectors of the crustal blocks by a non-linear inversion method [Matsu'ura and Hasegawa, 1987]. As prior information, an initial value for each unknown parameter was applied in the inversion. Initial parameter values are based on the results of previous studies of interplate coupling along the Suruga [Sagiya, 1999; Ohta et al., 2004] and Sagami [Sagiya, 2004] troughs, and previously estimated Euler vectors [Henry et al., 2001; Mazzotti et al., 2001; Altamimi et al., 2002; Sella et al., 2002]. Without applying the constraints, we found unrealistically high slip-deficit rates on offshore faults in the inversions. It is well known that geodetic data do not have much resolving power for slip on offshore faults far from observation points [e.g. Sagiya and Thatcher, 1999].

We assume there are four crustal blocks, each of whose movement is represented by a Euler vector (Figure 7). The Pacific and the Philippine Sea plates are subducting from the Japan trench and the Sagami and the Suruga troughs beneath central Japan, respectively. The Kanto and the Tokai regions are assumed to be part of a single block referred as the Central Japan block (CJP), although the Itoigawa-Shizuoka Tectonic Line (Figure 1b) is sometimes proposed as a plate boundary between eastern (Kanto) and western (Tokai) Japan.

Because recent GPS data [Sagiya, 2000] and historical triangulation data [Hashimoto and Jackson, 1993] suggest that the significant boundary for the contemporary deformation is not the Itoigawa-Shizuoka Tectonic Line but the Niigata-Kobe Tectonic Zone (Figure 1b), we do not separate the Central Japan block. Heki and Miyazaki (2001) studied the regional long-term deformation based on GPS data and concluded that the Tokai and Kanto regions move as predicted

by the North American plate. In accord with this view, geomorphological studies suggest that the slip rates of active faults along the southern part of the Itoigawa-Shizuoka Tectonic Line bounding Kanto and Tokai regions are very low [Research Group for Active Faults of Japan, 1991].   Finally, the majority of our geodetic observations lie to the east of the Itoigawa-Shizuoka Tectonic Line and the Niigata-Kobe Tectonic Zone (ISTL and NKTZ in Fig. 1b), and so our results are not strongly influenced by whether these low-slip-rate inland fault systems demark block boundaries.

The Izu peninsula, the northernmost part of the Izu-Ogasawara arc, was part of the Philippine Sea plate 2 million years ago and now is considered to be an independent micro-plate called the Izu micro-plate (IMP) by many researchers [e.g. Hashimoto and Jackson, 1993; Mazzotti et al., 1999, 2001; Sagiya, 1999; Heki and Miyazaki, 2001; Henry et al., 2001].   However, the eastern boundary of the IMP is proposed in various ways.   We regard the West Sagami Bay Fracture [Ishibashi, 2004] that extends in the north-south direction between the Izu Peninsula and Oshima Island as the eastern boundary of the IMP (Figure 2).   We assume a simple geometry of southern extension of the West Sagami Bay Fracture, following an alignment of earthquakes (Figure 2) west Niijima and Kouzushima (DD, EE and FF in Figure 7).   However, ours is not a unique solution, as seismicity around these islands is diffuse and previous studies [Mazzotti et al., 1999, 2001; Heki and Miyazaki, 2001] proposed several microplate boundary locations.   Geomorphological information such as active faults is insufficient to constrain the fault dip along the eastern boundary of the IMP, so we assume a simple geometry comprised of high-angle west-dipping faults.   Our geodetic data do not constrain the southern boundaries of the microplate (south of faults U and FF in Figure 7).

The geometry of fault and volcanic sources we employ is based on geological and seismological observations, and we use the geodesy principally to estimate the seismic and aseismic slip rate on these sources. These observations include the distribution of microseismicity, large (M≥6.5) and great (M≥7.9) earthquakes, and the distribution of Quaternary faults (Fig. 2), focal mechanisms (Fig. 13), Euler poles (Fig. 14), active volcanoes (Fig. 7), and bathymetry (Fig. 1b). We place the northwestern boundary of the Izu Microplate through the Fujigawa fault system (fault Z in Figure 7) and the southern flank of Mt. Fuji.   We identify fault patches on the Philippine Sea plate subducting from the Suruga trough and the Pacific plate subducting from the Japan trench following Ishida (1992), which was estimated from bathymetry, relocated hypocenters, and focal mechanism data.   For the Philippine Sea plate subducting from Sagami trough, we use the fault geometry estimated from seismic reflection profiling [Sato et al., 2005] and seismicity [Toda et al., 2006] with some modification.   We assumed upper and lower depths (e.g. locking depth) of the boundary faults in the subduction zones following Sagiya (1999, 2004).   The vertical depth of the

faults ranges from 10 to 85 km along the Japan trench, from 3 to ~40 km for the Sagami trough, and from 2 to ~20 km for the Suruga trough. The faults on the eastern and northwestern boundary of the IMP are assumed to extend between depths of 1-15 km.

The locations of all 32 faults are plotted in Figure 7 and their parameters are listed in Table 1. The assumption that fault G bounds CJP and PHS rather than the IMP was made because the PHS subducts near the triple junction; due to the proximity to the IMP Euler pole, the CJP-IMP relative motion at fault G is nearly zero. The rupture area and slip direction of the 1923 Kanto earthquake [Nyst et al., 2005] support the hypothesis that PHS is subducting on faults G and H, as these sources slipped in 1923. Therefore, we assigned G and H as bounding the CJP and the PHS, rather than the IMP. Some vertical steps and lateral discontinuities of the fault patches result from our approximation and simplification of the curved surfaces of subducting plate boundaries by planar rectangles. Since the geodetic data lie at the earth's surface, these incidences of overlap and underlap of fault patches has a negligible influence on the deduced seismic slip rates and coupling coefficients.

Six active volcanoes were modeled as point inflation sources; these include Mt. Fuji, eastern Izu, Oshima, Niijima, Kouzushima, and Miyakejima volcanoes. All of these volcanoes have erupted since the Ninth century. The most recent eruption of Niijima and Kouzushima occurred in AD 838; the most recent eruption of six volcanoes was the AD 2000 Miyakejima sequence [Nishimura et al., 2001; Toda et al, 2002]. Here we assume that the rate of magma intrusion at these volcanoes is constant, which permits us to isolate the tectonic strain associated with the fault sources

Except for the Eastern Izu volcanoes, there are no significant earthquakes or eruptions during the period we use to define the interseismic strain. For the initial point sources, we used parameters from Tada and Hashimoto (1991) for the eastern Izu volcanoes, GSI (2002) for the Oshima volcano, Nishimura et al. (2002) for Miyakejima volcano, and Kimata et al.(2000) and Nagoya University et al. (1999) for the Niijima and the Kouzushima volcanoes. We fixed the location and depth for Miyakejima; only the depth is fixed for Oshima and the eastern Izu volcanoes; for Niijima and Kouzushima, we estimated the location and depth in the inversion. Though GPS baselines extend across Mt. Fuji [e.g. Itani and Ishibashi, 2003], there are no quantitative models for the deformation source, so we assumed the location of the point source is 15 km below the summit, at the depth where low-frequency earthquakes have episodically occurred in 2000 and 2001 [Nakamichi et al., 2004]. The parameters of the point inflation sources are summarized in Table 2.

4. Inversion procedure and model misfit

We first tried to invert for a slip deficit rate for all faults with weak a priori constraints, and found that the estimated rate was unrealistically large and unstable for offshore Pacific plate megathrust patches C-F (the sources south of the 1938 rupture zone), and for patch T (the easternmost segment of the PHS). So we set the slip-deficit rate on the PAC segments to zero, and tightly constrained the slip rate on the easternmost segment of the PHS.   The Euler vector of the Pacific plate is fixed to be (63.1ºN, 79.2ºW, -0.919°/m.a.) [Altamimi et al., 2002] in the coordinate set (latitude, longitude, angular velocity), because there are no observation points on the Pacific plate.   Then, we inverted 524 GPS and 606 leveling observations to estimate the following unknowns: 28 slip-deficit rate parameters, 16 point sources of inflation, 9 Euler vectors, and 3 vertical reference points for the GPS and leveling data. Figure 8a shows the resulting slip-deficit rate estimated in the inversion; Tables 1 (faults), 2 (volcanoes), and 3 (Euler vectors) contain the full results.   The resolution shown in Figure 8c and listed in Tables 1 and 2, following Matsu'ura and Hasegawa (1987), represents the fraction of information provided by the observed geodetic data for each parameter.   As the resolution approaches 100%, the parameter estimates are resolved by the data and are insensitive to the initial parameters. The data resolution (Figure 8c) is a consequence principally of the non-uniform, or biased, distribution of the GPS network, and to a lesser extent on the diminished sensitivity of the GPS network to slip on the deepest fault sources. No segmentation boundaries are implied by the fault patch size; instead we have made the Pacific subduction sources larger because their resolution is so much lower than for the Philippine Sea plate sources.

The calculated horizontal GPS velocity vectors reproduce the observed vectors quite well (Figure 9).   Therefore residual horizontal velocity (Figure 10) is small in most areas.   The residuals are highest at some GPS stations in the Izu peninsula, the Izu islands, the Ogasawara islands, and the Daito islands.   The systematic misfit for the Ogasawara and the Daito islands implies an incorrect assumption for the Philippine Sea plate motion, which will be discussed in the next section.   The vertical GPS observations are generally matched by the best-fitting model (Figure 11); of greatest importance, the subsidence on the southern coast in the Tokai and Kanto regions are well reproduced by the model.   However, a large misfit in the Izu islands suggests that our kinematic model is too simple to explain the complex volcanic deformation. The reduced χ^2, that is, χ^2 per degree of freedom is defined as

$$\chi^2 = \frac{1}{(n-p)} \sum_{i=1}^{n} (\frac{r_i}{\sigma_i})^2$$

where n is the number of data, p is the number of parameters, r_i is the residual (the observed

minus calculated data), σ_i is the data uncertainty. A good model should have a reduced $\chi^2 \sim 1$ whereas the reduced χ^2 of our best-fitting model is 14.8. The average residual magnitude is 1.3 mm/yr for horizontal GPS, 2.6 mm/yr for vertical GPS, and 0.6 mm/yr for the leveling velocities. These magnitudes are several times larger than the data uncertainties used in this study. The likely reasons for the large reduced χ^2 is that unmodeled non-tectonic deformation has contaminated some of the observations, and that the assumed model fault geometry is not fully appropriate. An example of the former is short wavelength subsidence on routes 3 and 4 of leveling data (Figures 6c and 6d), and an example of the latter is the large misfit in the Daito and the Ogasawara islands (Figure 9). It is also possible that the data uncertainties are underestimated for our GPS data. The strategy of baseline analysis, and the conditions of GPS stations, including monument stability and atmospheric water vapor, may be different for the GEONET data and the U.S. data analyzed by Dixon et al.(2000).

5. Results and Discussion

5.1 Tests for the existence of an Izu microplate

There are several contentious or unresolved issues about the Kanto triple junction and plate geometry. For our best-fit model, Figure 12 shows the rigid block rotation, elastic deformation, and their sum in the CJP-fixed reference frame. Figure 13 shows the relative movement on block boundary faults calculated from the Euler poles of the best-fit model. This relative movement can be interpreted as a long-term slip rate of the faults averaged over many earthquake cycles. The slip-deficit rate represents the part of this movement that is presumed to be episodic (e.g. seismic). Figure 14 shows a comparison of the location of the estimated Euler poles with that of the previous studies.

The first issue is whether the Izu peninsula moves, as we have assumed, as an independent crustal block. We combined the Izu micro-plate (IMP) and the Philippine Sea plate (PHS) as a single plate in the inversion, and found a reduced χ^2 2.3 times higher than that of the best-fit model. We therefore conclude that the IMP is necessary to explain the contemporary deformation. Although Hashimoto and Jackson (1993) and Hashimoto et al. (2000) suggest the Izu peninsula should be separated from the rigid part of PHS, the geometry of the block boundaries they proposed do not fully predict the observed deformation for these regions. Using geomorphological data, P-axes of earthquakes, and GPS data, Mazzotti et al.(1999, 2001) estimated the IMP Euler pole (Zenisu-West Izu Block). Henry et al. (2001) estimated the motion of the IMP down-going slab along the Suruga trough solely from GPS strain data. Our estimation for the IMP Euler pole with respect to the Eurasian plate is (36.6ºN, 139.0ºE, -10.0°/m.a.). Within the CJP reference frame,

the IMP Euler pole locates at (35.30°N, 139.05°E), near the boundary between IMP and CJP (Figures 11 and 13), and its angular velocity is high (-9.7°/m.a.). Although our result is roughly consistent with the rapid clockwise rotation estimated by Mazzotti et al.(1999, 2001) and Henry et al.(2001), our location and angular velocity are significantly different from theirs (36.4ºN, 139.8ºE, -5.6°/m.a.). This is probably because Henry et al. (2001) used GPS strain data only on the overriding plate to consider the elastic deformation, whereas we modeled GPS velocities on both sides of the Suruga trough, taking both elastic deformation and rigid motion into consideration. Our estimated pole fits the observed GPS velocities around the IMP better than those of previous studies. However, the geodetic data leave uncertainties of the IMP pole because the pole depends on the assumed area of the IMP near its southeastern boundary.   Furthermore, the southern boundaries of the IMP are not evident from seismicity and insufficiently sampled by GPS.

Here we speculate on what causes the rapid rotation of the IMP.   The northern part of the Izu-Ogasawara arc started to collide with central Japan ~15 Ma [e.g. Stern et al., 2004]. Geological evidence shows that the terrains north of the Izu peninsula (e.g. Tanzawa massif) were formerly part of the Izu-Ogasawara arc, and that they accreted onto central Japan.   Because the Izu peninsula, a former island, has a thick and buoyant crust, it cannot subduct beneath the CJP.   The history of the Ashigara Basin at the northern edge of the Izu peninsula suggest the peninsula has been colliding into the CJP for ~2 Ma [Soh et al., 1998].   Because of resistance to the collision, a new boundary south of the Izu peninsula formed to accommodate part of relative plate motion between the PHS and the CJP. In contrast, subduction along the Suruga trough, west of the Izu Peninsula, is still ongoing. Therefore the Izu peninsula (IMP) was prevented from moving northward and instead moves west. The northwestward-moving PHS pushes the IMP on its southeastern boundary.   This force, and the resistance of the northward movement at the northern boundary, cause the CJP to rotate rapidly clockwise.   Our hypothesis is consistent with the IMP rotation pole's location near the Ashigara Mountains, which act as a pivot point.   A similar rapid rotation of a plate due to a collision resistance force in or near a subduction zone was proposed for Papua New Guinea, New Zealand, Tonga, Vauatu, and Marianas by Wallace et al.(2004, 2005).

A limitation of this hypothesis stems from the absence of GPS vectors within the IMP except at its northern end and in the Izu peninsula. The vectors within Izu and along the Izu islands are partly contaminated by volcanic processes. Although the one IMP vector, for the Zenisu reef at 33.9°N/138.8°E, has a large residual, it is based on only two campaign measurements and its location is close to the presumed microplate boundary.   Paleomagnetic data or future additional GPS measurements for this reef or the other islands might permit one to independently validate the expected rotation rate.

Although we treat the IMP as a single elastic block, the residual velocity (Figure 10) suggests the possibility of diffuse deformation across the IMP. A left-lateral strike-slip fault system including the Tanna fault, which ruptured in the 1930 M=7.0 Kita-Izu earthquake [Abe, 1978], is a north-striking left-lateral fault in the northern and central part of the Izu Peninsula. The residual velocity suggests southward motion of the western half of the Izu peninsula, concordant with the left-lateral motion across the fault system. In the eastern part of the Izu Peninsula, large earthquakes have struck, including the M=6.9 1974 Izu Hanto-Oki [Abe, 1978] and the M=7.0 1978 Izu Oshima shocks. These right-lateral strike-slip earthquakes occurred on the faults striking east-west or ESE-WNW. The two fault systems are roughly conjugate, and imply that the motion between the IMP and the PHS in the eastern part of the Izu peninsula is distributed among several conjugate fault systems. Thus we favor a zone of distributed deformation including the eastern part of the Izu peninsula, Kouzushima, and Niijima, as first proposed by Mazzotti et al.(1999).

The relative velocity along the eastern boundary of the IMP is ~28 mm/yr of left-lateral motion. The direction of the relative motion is roughly parallel to the boundary near Kouzushima and Niijima as well as east off the Izu peninsula. The Euler poles of the previous studies [Mazzotti et al., 1999, 2001; Heki and Miyazaki, 2000; Henry et al., 2001] predict that the angle between the boundary and the relative motion is ~60º near Kozushima, which implies a large convergent component on the boundary. The focal mechanisms of shallow (depth < 30km) earthquakes determined by a waveform inversion [Fukuyama et al., 1998] are plotted in Figure 13. Most of the earthquakes near Kouzushima are strike-slip with one nodal plane approximately parallel to the boundary, consistent with our results. Although the West Sagami Bay Fracture (fault BB in Figure 7 and 8) was originally considered to be an intraplate fracture [Ishibashi, 2004], our result suggests it instead bounds the PHS and the IMP.

The long-term relative velocity ranges from 11 mm/yr to 25 mm/yr along the Suruga trough, where an M~8 earthquake has long been anticipated [e.g. Ando, 1975; Ishibashi, 1981]. Our result suggests that the convergence rate varies along the Suruga trough due to the rotation of the IMP. Heki and Miyazaki (2001) proposed that the convergence rate along the Suruga trough (~19 mm/yr) was one-third of that along the Nankai trough (~62 mm/yr). Our results support the small convergence rate along the Suruga trough.

The southwestern boundary of the IMP (light dashed line in Figure 7) cannot be constrained by the geodetic data due to the limited coverage of the geodetic observation points. Neither bathymetry (Figure 1b) nor seismicity (Figure 2) shows clear alignments along the boundary, leaving the southwestern boundary of the IMP uncertain. The 2004 off-Kii peninsula M=7.4 earthquakes [e.g. Satake et al., 2005] occurred near the southwestern boundary. Their epicenters

are plotted near the southwestern corner of Figure 2.   Henry (2004) proposed that the 2004 off Kii peninsula earthquakes occurred on the boundary between the PHS and IMP.   This is because the thrust faulting with east-west strike of the earthquakes is explained by the relative Euler poles between the PHS and IMP estimated by Henry et al. (2001) and Mazzotti et al.(2001).   The relative pole estimated in this study is not consistent with the focal mechanisms of the off Kii peninsula earthquakes.   It is still controversial whether the 2004 off Kii peninsula earthquakes that ruptured both strike-slip and thrust faults [e.g. Satake et al., 2005; Hara, 2005] are related to the Izu microplate.

5.2   Configuration and movement of CJP and PHS

A central issue for the tectonics of Japan is to assess which plate the inland Kanto and Tokai regions belongs to.   Though these regions were classically considered as two distinct plates separated by the Itoigawa-Shizuoka Tectonic Line (Figure 13), we treated these regions as one crustal block (CJP) based on recent studies of GPS velocity field [Sagiya et al., 2000; Mazzotti et al., 2001; Heki and Miyazaki, 2001].   The Euler vector for the Central Japan block (CJP) is estimated to be (75.9ºN, 130.9ºE, –0.351°/m.a.) with respect to the Eurasian plate. Because the residual velocity field (Figure 10) does not show systematic features, the single-plate assumption is sufficient to represent the contemporary deformation of the greater Kanto region, given the limited geodetic data we consider southwest of the ISTL.   But because of large uncertainties of the CJP Euler vectors, we cannot determine whether the CJP belongs to the North American, the Okhotsk, or an independent plate.   The estimated CJP pole relative to the Eurasia plate differs little from the North American plate (73.0 ºN, 129.0 ºE, -0.248°/m.a. [Altamimi et al., 2002] or 68.1 ºN, 136.4 ºE, -0.245 °/m.a. [Sella et al., 2002]), or for the Okhotsk plate (61.8 ºN, 143.3 ºE, -0.546 °/m.a. [Sella et al., 2002]).   Because the estimated CJP pole is far from the Kanto region and the area of the CJP is rather small, all geodetic sites on the CJP translate in parallel with little rotation. Near Tokyo (35.7 ºN, 139.7 ºE), the CJP pole predicts a velocity of 25 mm/yr oriented 257º with respect to the EUR. This velocity is similar to the 27 mm/yr oriented 274º predicted for the Okhotsk plate [Sella et al., 2002], but differs significantly from the 15-17 mm/yr oriented 265-268º predicted for the North American plate [Altamimi et al., 2002; Sella et al., 2002].

The estimated location of the PHS Euler pole (45.8ºN, 150.6ºE, -1.592°/m.a) is compared with that of previous studies in Figure 14.   The poles of REVEL [Sella et al., 2002] and Seno et al.(1993) were estimated from GPS velocity and earthquake slip vectors, respectively.   Though poles of both our study and Sella et al. (2002) are estimated from GPS data, the locations are significantly different because we included the Izu Islands vectors.   Our Euler pole predicts the

15

motion of the Izu islands well but does not do so for the Daito and the Ogasawara islands.

We tested the case of the PHS Euler vector the REVEL pole (Figure 15). The REVEL Euler pole explains the motion of the Daito and the Ogasawara islands but predicts a residual ~10 mm eastward movement of the Izu islands. Because the Izu islands are a chain of volcanic islands, local volcanic sources may contaminate, if not cause, the deformation. Another explanation is that the eastward residual velocity of the Izu islands in the REVEL prediction is caused by back-arc or inter-arc spreading west of the Izu islands, and that our Euler pole represents the forearc of the Izu islands rather than the motion of the Philippine Sea plate. The relative Euler vector between REVEL and ours predicts 9 mm/yr of divergence at 34ºN and 139.3ºE in the east-west direction. This divergence is consistent with the existence of an inter-arc rift basins just west the Izu islands [Stern et al., 2004]. The long-term relative motion along the Sagami trough between PHS (possibly the forearc of the Izu islands) and CJP is oriented N16-23ºW with a rate of 22-27 mm/yr (Figure 13 and Table 1). This orientation is also different from REVEL by ~10º. Comparing Figures 12 and 15, our Euler vector explains the deformation near the Sagami trough better than that of REVEL. Sagiya (2004) pointed out that the slip-deficit vectors along the Sagami trough deviated from the prediction of REVEL by 10º, which is concordant with our result.

5.3 Characteristics of seismic portion of fault slip rate for hazard analysis

Here we discuss the distribution of the seismic portion of the slip rate (the 'slip-deficit' rate) to determine how strongly each fault patch is coupled, to estimate its seismic moment accumulation rate and, to compare the patches where the slip-deficit is appreciable to the rupture areas of past large earthquakes. The slip-deficit rate (Figure 8a) is that part of the long-term fault slip rate that is inferred to be locked and therefore presumed to produce large earthquakes. We thus regard the slip-deficit rate as the seismic, or at least episodic, portion of fault slip rate. Figure 8b shows the coupling coefficient, which is ratio of the seismic portion of fault slip rate to the long-term slip rate (Figure 13). A coupling coefficient of 0 indicates a fault is creeping at its long-term rate; a coupling coefficient of 1 indicates that the fault is fully locked and thus building strain to be released in earthquakes or episodic creep.

We assumed the vertical depth of the fault patches ranges from an upper depth of 3 km to a maximum lower depth of 40 km along the Sagami trough beneath the Kanto. The seismic portion of slip rate along the Sagami trough is great on the faults shallower than 20 km and still significant at the depth of 20-40 km. The 1923 Kanto earthquake ruptured the region of faults G-J, L, and M [Wald and Somerville, 1995, Nyst et al., 2005; Sato et al, 2005], where the seismic portion of slip rate ranges from 12 to 40 mm/yr. A peak of the rate (40 mm/yr) is found on fault L beneath the tip

of the Boso peninsula, which corresponds to one of two peaks of coseismic slip in the 1923 earthquake [Wald and Somerville, 1995; Pollitz et al., 2005; Sato et al, 2005]. The seismic portion of slip rate is not as high (18 mm/yr) on fault G where the other peak of the coseismic slip locates.

The seismic portion of slip rate is also high (40-47 mm/yr) on faults P-R off and southeast of the Boso peninsula, which did not rupture in 1923 but did slip in the M~8.2 1703 Genroku Kanto earthquake, as inferred from uplifted marine terrace and tsunami run-up data. Several authors [e.g. Ishibashi, 1977; Matsuda et al., 1978; Shishikura 2003] argued that the 1703 shock ruptured both the source area of the 1923 earthquake and also its southeastern extension. The 1703 rupture models estimated from coseismic vertical displacement [Shishikura, 2003] and tsunami inundation heights [Murakami and Tsuji, 2002] leave uncertain how far the rupture area extended to the southeast, but both involve sources resembling fault P and they might have also involve sources resembling Q and R. Matsuda et al. (1978) and Shishikura(2003) proposed that the 1703 earthquake ruptured a high-angle reverse fault near the southern tip of the Boso peninsula. If the proposed fault has a large slip rate and is locked in the interseismic period, a sharp subsidence of the southern tip of the Boso Peninsula is expected. However, there is no significant deformation on leveling route 7 (Figures 3 and 6g), making the existence of strain accumulation on such a high-angle fault unlikely. Therefore, we did not include the fault proposed by Matsuda et al.(1978) and Shishikura(2003).

There are several points to consider regarding whether an earthquake would rupture faults P, Q, R, and T in the future. First, the seismic portion of slip rate on faults Q and T is not resolved by the observed data (Figure 8c; Table 1). If the rate on fault T is fixed to be zero, the rate on fault R increases by 10 mm/yr, which is unreasonably high for the convergence rate along the Sagami trough. Therefore, some coupling must exist on fault T. The seismic portion of the slip rate on faults surrounding fault Q are insensitive to the slip assigned to fault Q, which means the observed data cannot resolve the slip deficit rate on fault Q.

Fault R may be a special case, because it exhibits episodic slow slip events rather than purely locked behavior. Slow slip events with an equivalent moment magnitude of ~6.5 were detected by GPS in the Boso peninsula in 1996 and 2002 [Ozawa et al., 2003; Sagiya 2004] (dashed ellipse in Figure 13). Ozawa et al. (2003) suggested that the 1996 and 2002 events have similar focal areas and slip process. The 2002 event has approximately 200 mm of slip over an area of 35×35 km^2, which coincides with fault R. Ozawa et al.(2003) proposed a 6-7 year recurrence interval for slow slip events similar to those in 1996 and 2002, amounting to a slip rate of ~30 mm/yr. Because the inferred rate is 42 mm/yr on fault R, most of this slip might be released episodically by creep events.

Our overall pattern of seismic slip rate and coupling distribution along the Sagami and Suruga troughs resembles Sagiya (2004) and Ohta et al. (2004). Along the Suruga trough, the estimated rate on fault U is larger than the that of Ohta et al. (2004), but our rate is likely unrealistic because fault U locates on the edge of the study area. Along the Sagami trough, the slip-deficit rate estimated in this study is generally larger than that of Sagiya (2004). A significant slip-deficit rate of 18 mm/yr is found on fault O beneath the eastern part of the Boso peninsula, where the rate is almost zero in Sagiya (2004). Coupling on fault O (Figure 8b) may suggest it was the site of the 2005 M=6.0 Chiba earthquake and the M~7 1855 Ansei Edo earthquake [Bakun, 2005; Grunewald and Stein, 2006].

We fixed the seismic portion of slip rate to zero in the southern part of the subducting Pacific plate (faults C-F) and estimated the rate on faults A and B because of limited data resolution for these sources, leading to negative rates when they are not fixed. We infer from this that faults C-F may be freely slipping and thus seismically uncoupled, but we recognize the limitations on this inference. Fault A, site of the 1938 M=7.5, 7.4, and 7.3 earthquake swarm [Abe, 1977], has a high seismic slip rate (68 mm/yr), which implies strong coupling, a rate higher than implied by its historical seismic record. The resulting 4 m of accumulated deficit on the 100×150 km span of fault A implies a current seismic potential of 1.9×10^{21} Nm, or M_W~8.1. Nishimura et al.(2004) also estimated that the interplate coupling on the northern extension of faults A and B is strong.

A high seismic portion of slip rate is inferred along the eastern boundary of the IMP, although the rate of 77 and 59 mm/yr on fault DD and EE is unrealistic and likely contaminated by unmodeled volcanic deformation around Niijima and Kouzushima. The fault BB exhibits rates of 29 mm/yr, which means its coupling coefficient is nearly 1 (Figure 8a and 8c). This suggests that these faults are completely locked and have a large seismic potential. From the 17th Century through 1923, large earthquakes have struck Odawara about every 70-80 years [Ishibashi, 2004]. Since the last such event in 1923, the accumulated deficit would be 2.2 m over a fault 35 km $\times$ 15 km in extent, yielding a moment of 3.5×10^{19} Nm, or M_W=7.0. Thus, fault BB, and perhaps fault G, are likely candidates for the frequent and damaging Odawara earthquakes. In contrast, fault CC has a low seismic rate of 5 mm/yr. It ruptured in the 1980 M=6.7 Izu-Hanto Toho-Oki earthquake, and several large earthquakes (M~6) have since occurred there in 1990's. The small seismic rate implies that postseismic transients may have occurred during 1996-2000.

Grunewald and Stein (2006) compared the moment rate released by historical earthquakes since 1649 to the moment accumulation rate inferred from this study, and found them to be in close agreement. This suggests that the secular strain rate measured over the past decade is in fact representative of the longterm process, under the assumption that the earthquake catalog is

18

sufficiently long. At the very least, the catalog is 100 times longer than the geodetic time series we use here.

5.4 Estimated Volcanic Inflation

Are all the volcanic sources necessary to satisfy the observations, and does their inclusion permit us to gain more insight into the nearby tectonic faults? We tested the improvement of the data fit caused by each inflation point and found all six inflation sources to be statistically significant in reducing the misfit, accounting for the number of parameters with the AIC (Akaike Information Criterion) and F-test [e.g. Stein and Gordon, 1984]. The reduced χ^2 with and without the six inflation sources are 14.8 and 19.8, respectively. The improvement associated with Mt. Fuji is the smallest of all the volcanoes, and the reduced χ^2 without Mt. Fuji is 15.0. However this improvement is still significant at the 99.99 % confidence level of the F-test.

The highest inflation rate is inferred for Miyakejima, which erupted in 2000, just after the end of the observation period (Table 2). A high inflation rate is inferred for the eastern Izu volcanoes, which erupted in 1989 [Tada et al., 1991] and caused episodic dike intrusions shown in Figure 4b [e.g. Aoki et al., 1999]. It is notable that the Niijima volcano, which has sustained no eruption during the past 1200 years, has an inflation rate of $3.2 \times 10^6 \, \mathrm{m}^3$/yr, and thus has a large potential for a future eruption. The inflation source beneath Kouzushima is at a depth of only 1.3 km. We are certain that the source is shallow because the vectors of three GPS stations on Kouzushima point outward (Figures 5 and 9). But because of the large misfit on Kouzushima (Figure 10), as well as the unrealistic slip-deficit rate on fault EE, we are not confident about this depth and inflation rate. Because of high sensitivity to the assumed depth, the inflation rate of $3.9 \times 10^6 \, \mathrm{m}^3$/yr beneath Mt. Fuji is not well constrained. But Mt. Fuji is clearly inflating, and magma is thus accumulating beneath the largest volcano of Japan, whose last eruption was in 1707. If this rate were constant, then ~1.2 km^3 of magma might have since accumulated, roughly double the eruptive volume in 1707 of ~0.7 km^3 [Miyaji, 1988].

5.5 Limitations of the analysis and future research

We used geodetic data spanning ~4 years to estimate the present kinematics of central Japan under the assumption that the deformation rate is constant. However, time-dependent and episodic deformation are observed by the continuous geodetic network and by tiltmeters. One example is the occurrence of slow slip events near Tokai and east of the Boso peninsula [Ozawa et al., 2002, 2003; Ohta et al., 2004; Sagiya, 2004]. Another example is volcanic deformation that is known to change with time. For example, Nishimura et al.(2002) reported that the deformation rate of

Miyakejima significantly changed in the magma accumulation period between the 1983 and 2000 eruptions.   Vertical displacement observed by repeated leveling surveys for the past 100 years suggests the volcanic inflation for the eastern Izu volcanoes were episodically active in 1930's, 1980', and 1990's [Geographical Survey Institute, 2005].   Therefore, we have tried to validate our assumption of uniformity wherever possible, exclude non-secular data when it could be so identified. Further validation would nevertheless build confidence in our inversion results as to the accumulated slip deficit and the volume of accumulated magma. A longer geodetic record would also be invaluable if the 2000 Izu Islands swarm and post-swarm transients could be properly removed from the time series.

The estimated seismic portion of the fault slip rate exceeds the relative block motion on a couple of faults (in other words, the seismic coupling coefficients exceed 1), which is physically unreasonable. There are several possible sources for this error.   First, the slip rate near the edge of the studied area such as faults U and EE may be overestimated by neglecting the sources just outside.   Second, the assumed boundaries of the crustal blocks, including fault geometry and location, may not be appropriate in some cases.   For example, in the volcanic area around Niijima and Kouzushima, the seismic portion of fault slip rate on faults DD and EE are more than twice the long-term slip rate, and so our model is too simple to explain the complicated deformation in that area.   Offshore faults such as P, Q and R along the Sagami trough also have high seismic portion of their slip rates.   We tested two geometries of the subducting PHS proposed by Ishida(1992) and Sato et al.(2005), and we adopted the geometry of Sato et al(2005) because of its smaller misfit. But the slip rates of the offshore faults are unreasonably high for both geometries.   Lallemant et al.(1996) suggested that a tectonic sliver including the southern tip of the Boso and the Miura peninsulas is bounded by the right-lateral fault extending approximately 150 km from the Miura peninsula through the Boso peninsula and out to the ocean (the 'Boso transform fault' in Figure 1b). Pollitz et al.(2005) suggests a part of the Boso transform faults ruptured in the 1923 Kanto earthquake.   Although the introduction of the sliver reduces the seismic portion of slip rate along the Sagami trough, the small number of the GPS stations south of the Boso transform fault makes it difficult to assess this hypothesis and include it stably in the inversion.

Recently, a seismic experiment to investigate the fault geometry of the megathrust fault that ruptured in the 1923 earthquake [Sato et al., 2005] showed the subduction interface branches to the surface near the westernmost portion of the Sagami trough.   One branch is similar to the geometry of fault G.   The other is the high-angle reverse Kouzu-Matsuda fault, whose geological slip rate is one of the highest (~3 mm/yr) among the active faults in Japan [Research Group for Active Faults of Japan, 1991]. The complex fault geometry needed to incorporate fault branching and slip

partitioning was not modeled in this study and thus it absence may cause a systematic error in the slip-deficit estimation.   A third source of the modeling error is the assumption of the homogeneous elastic half-space to calculate the surface displacement.   The Kanto Basin contains up to 3 km of sediment [Yamanaka and Yamada, 2002].   A weak surface layer with low elastic modulus makes surface displacements due to buried dislocation larger than that of a homogeneous medium [e.g. Pollitz, 1996], which can lead to overestimation of the seismic portion of slip rate.

Another source of modeling error is that we do not consider inelastic deformation.   In our analysis, we assume that the interseismic elastic deformation will be cancelled out by the coseismic deformation, leaving only rigid block-motion remaining in long term, and deformation due to body forces (buoyancy, sedimentation, and erosion).   The marine terraces developed in the tips of the Boso and Miura peninsulas are evidence of permanent secular deformation. Shishikura (2003) estimated 13 m of uplift during the past 6800 years, that is, ~2 mm/yr in the southern tip of the Boso peninsula.   The rapid secular uplift in the tips of the peninsulas cannot be explained by simple block motion and may suggest plastic deformation or the movement of complex splay faults near the troughs.   Stein et al.(2006) compared the inter-event time for M~8 earthquakes along Sagami trough from observations of the marine terrace record with that estimated from our slip-deficit rate and coseismic slip for the 1923 Kanto and 1703 Genroku earthquakes.   They found that geodetic estimation of the inter-event time (~250 years) is significantly smaller than that from marine terrace record (403±66 years). This may hint at time-dependent strain accumulation and unmodeled deformation caused by complex fault geometries and inelasticity, which should be included in the future analyses.

6. Conclusion

The block-fault model, including point inflation sources, successfully reproduces the contemporary deformation of the Kanto region, the eastern Tokai and the Izu regions, and the southwest portion of central Japan observed by GPS and leveling during 1996-2000.   We argue for the existence of the Izu micro-plate, and find that it rotates clockwise with respect to the Central Japan block rapidly (9.7º/m.a.).   Because the pole and angular velocity of the microplate are dependent on the assumed plate configuration, additional continuous GPS observations or paleomagnetic data would be invaluable to confirm this hypothesis. The pole of the rotation locates near the boundary between the proposed Izu micro-plate and the Central Japan block, which we interpret as a pivot point between two blocks.   A high seismic portion of slip rate (12-48 mm/yr) along the Sagami trough is estimated not only for the fault segments that ruptured in the 1923 M=7.9 Kanto earthquake, but also in the region southeast of the Boso peninsula that last ruptured in

the 1703 M~8.2 shock, suggesting strong plate coupling.   Though episodic creep events occurred on nearby faults in 1996 and 2002, they released only part of the accumulated stress in a restricted area east of the Boso peninsula, and so the broader region still has a high seismic potential.   The seismic portion of slip rate along the Suruga trough decreases to the north, consistent with the relative block motion predicted by the rotation of the Izu micro-plate.   Along the Pacific plate, only the portion of the megathrust that ruptured in the 1938 earthquake swarms is clearly fully coupled and thus known to be accumulating strain. The coupling is unresolved on the downdip extension of the 1938 zone and all of the Pacific plate to the south, and so there the seismic slip rate cannot be determined. The eastern boundary of the Izu micro-plate, including the West Sagami Bay Fracture, has a left-lateral slip motion and is currently locked except where the 1980 M6.7 Izu-Hanto-Toho-Oki earthquake struck.

Reference

Abe, K. (1977), Tectonic implications of the large Shioya-Oki earthquakes of 1938, *Tectnophysics, 41*, 269-289.

Abe, K. (1978), Dislocations, source dimensions and stresses associated with earthquakes in the Izu peninsula, Japan, *J. Phys. Earth*, *26*, 253-274.

Altamimi, Z., P. Sillard, and C. Boucher (2002), ITRF 2000: A new release of the International Terrestrial Reference Frame for earth science applications, *J. Geophys. Res*, *107*(B10), 2214, doi:10.1029/2001JB000561.

Ando, M. (1971), A fault-origin model of the great Kanto earthquake of 1923 as decuced from geodetic data, *Bull. Earthq. Res. Inst., Univ. Tokyo*, *49*, 19-32.

Ando, M. (1975), Possibility of a major earthquake in the Tokai district, Japan and its pre-estimated seismotectonic effects, *Tectonophysics, 25*, 69-85.

Aoki, Y., P. Segall, T. Kato, P. Cervelli, and S. Shimada (1999), Imaging magma transport during the 1997 seismic swarm off the Izu Peninsula, Japan, *Science*, *286*, 927-930.

Bakun, W. H. (2005). Magnitude and location of historical earthquakes in Japan and implications for the 1885 Ansei Edo earthquake, *J. Geophys. Res., 110*, No. B2, B02304, doc:10.1029/2004JB003329.

Dixon, T.H., M. Miller, F. Farina, H. Wang, and D. Johnson (2000), Present-day motion of the Sierra Nevada block and some tectonic implications for the Basin and Range province, North American Cordillera, *Tectonics*, *19*, 1024.

Fukuyama, E., M. Ishida, D. S. Dreger, and H. Kawai (1998), Automated seismic moment tensor determination by using on-line broadband seismic waveforms, (in Japanese with English abstract), *Zisin (J. Seismol. Soc. Jpn.)*, *51*, 149-156.

Geodetic Observation Center (2004), Special Issue: Establishment of the nationwide observation system of 1200 GPS-based control stations (in Japanese), *J. Geograph. Surv. Inst.*, *103*, 1-51.

Geographical Survey Institute (1999), Report on survey and investigation of land subsidence in the Kanto region (in Japanese), *Technical Rep. Geograph. Surv. Inst.*, B.7-F-No16, 23 pp.

Geographical Survey Institute (2002), Crustal movements in the Izu peninsula and its vicinity (in Japanese), *Rep. coordinating committee for earthquake prediction*, *68*, 200-229.

Geographical Survey Institute (2005), Crustal movements in the Izu peninsula and its vicinity (in Japanese), *Rep. coordinating committee for earthquake prediction*, *74*, 176-229.

Grunewald, E. D., and R. S. Stein (2006), A new 1649-1884 catalog of destructive earthquakes near Tokyo and implications for the long-term seismic process, J. Geophys. Res, in press.

Hara, T. (2005), Change of the source mechanism of the main shock of the 2004 off the Kii

peninsula earthquakes inferred from long period body wave data, *Earth Planets Space*, 57, 179-183.

Hashimoto, M., and D. D. Jackson (1993), Plate tectonics and crustal deformation around the Japanese islands, *J. Geophys. Res*., *98*, 16149-16166.

Hashimoto, M., S. Miyazaki, and D.D. Jackson (2000), A block-fault model for deformation of the Japanese Islands derived from continuous GPS observation, *Earth Planets Space*, *52*, 1095-1100.

Heki, K., and S. Miyazaki (2001), Plate convergence and long-term crustal deformation in central Japan, *Geophys. Res. Let*., *28*, 2313-2316.

Henry, P., S. Mazzotti, and X. Le Pichon (2001), Transient and permanent deformation of central Japan estimated by GPS, 1. Interseismic loading and subduction kinematics, *Earth. Planet. Sci. Let*., *184*, 443-453.

Henry P., (2004), Intraplate deformation southeast off Kii Peninsula, Mini-symposium on 2005/09/05 Offshore southeast of the Kii Peninsula earthquakes, Japan Agency for Marine-Earth Science and Technology, Yokosuka, Japan, 13 Oct.

Ishibashi, K. (1977), Source region of the 1703 Genroku Kanto earthquake and recurrence time of major earthquakes in Sagami Bay, Japan (1) (in Japanese), *Zisin (J. Seismol. Soc. Jpn.), 30*, 369-374.

Ishibashi, K. (1981), Specification of a soon-to-occur seismic faulting in the Tokai district, central Japan, based upon seismotectonics, in *Earthquake Prediction, An International Review, Maurice Ewing Ser.*, vol. 4, Edited by D. W. Simpson and P. G. Richards, pp. 297-332, AGU, Washington, D. C.

Ishibashi, K. (2004), Seismotectonic modeling of the repeating M7-class distrous Odawara earthquake in the Izu collision zone, central Japan, *Earth Planets Space, 56*, 843-858.

Ishida, M. (1992), Geometry and relative motion of the Philippine Sea Plate and Pacific plate beneath the Kanto-Tokai district, Japan*, J. Geophys. Res., 97*, 489–513.

Itani, Y., and K. Ishibashi (2003), Horizontal crustal strain in the Izu Peninsula-Mt. Fuji region derived from GEONET data and its tectonic implication (in Japanese with English abstract), *Zisin (J. Seismol. Soc. Jpn.),* 56, 231-243.

Kanamori, H. (1971), Faulting of the great Kanto earthquake of 1923 as revealed by seismological data, *Bull. Earthq. Res. Inst., Univ. Tokyo*, *49*, 13-18.

Kimata, F., S. Kariya, M. Fujita, K. Matsumoto, T. Tabei, J. Segawa, and A. Yamada (2000), Estimated pressure source on Kozu Island volcano, South Central Japan, from GPS measurements (July 1996-August 1999), *Earth Planets Space*, *52*, 975-978.

Lallemant, S. J., X. Le Pichon, F. Thoue, P. Henry, and S. Saito (1996), Shear partitioning near the central Japan triple junction: the 1923 great Kanto earthquake revisited - I, *Geophys. J. Int., 126*, 871–881.

Mao, A., C. G. A. Harrison, and T. H. Dixon (1999), Noise in GPS coordinate time series, *J. Geophys. Res., 104*, 2797-2816.

Matsuda, T., Y. Ohta, M. Ando, and N. Yonekura (1978), Fault mechanism and recurrence time of major earthquakes in southern Kanto district, Japan, as deduced from coastal terrace data, *Geol. Soc. Am. Bull., 89*, 1610-1618.

Matsu'ura, M., T. Iwasaki, Y. Suzuki, and R. Sato (1980), Statical and dynamical study on faulting mechanism of the 1923 Kanto earthquake, *J. Phys. Earth, 28*, 119-143.

Matsu'ura, M., D. D. Jackson, and A. Cheng (1986), Dislocation model for aseismic crustal deformation at Hollister, California, *J. Geophys. Res., 91*, 12661-12674.

Matsu'ura, M. and Y. Hasegawa (1987), A maximum likelihood approach to nonlinear inversion under constraints, *Phys. Earth Planet. Inter., 47*, 179-187.

Mazzotti, S., P. Henry, X. Le Pichon, and T. Sagiya (1999), Strain partitioning in the zone of transition from Nankai subduction to Izu-Bonin collision (Central Japan): implications for an extensional tear within the subducting slab, *Earth. Planet. Sci. Lett., 172*, 1-10.

Mazzotti, S., P. Henry, and X. Le Pichon (2001), Transient and permanent deformation of central Japan estimated by GPS, 2. Strain partitioning and arc-arc collision, *Earth. Planet. Sci. Lett., 184*, 455-469.

McCaffrey, R. (2002), Crustal block rotations and plate coupling, in *Plate Boundary Zones, Geodyn. Ser.*, vol. 30, edited by S. Stein and J. Freymueller, pp. 101-122, AGU, Washington, D. C.

Meade, B. J., B. H. Hager, S. C. McClusky, R. E. Reilinger, S. Ergintav, O. Lenk, A. Barka, and H. Özener (2002), Estimates of seismic potential in the Marmara Sea Region from Block Models of Secular Deformation Constrained by Global Positioning System Measurements, *Bull Seismol. Soc. Am., 92*, 208-215.

Miyaji, N. (1988), History of Younger Fuji Volcano (in Japanese with English abstract), J. Geol. Soc. Jpn., 94, 433-452.

Mogi, K. (1958), Relations between the eruptions of various volcanoes and the deformations of the ground surfaces around them, *Bull. Earthq. Res. Inst., Univ. Tokyo, 36*, 99-134.

Murakami, Y., and Y. Tsuji (2002), Fault model of the Genroku Kanto Earthquake of December 31, 1703 estimated by the distribution of the tsunami heights (in Japanese), *Kaiyo Monthly, Extra 28*, 161-175.

Nagoya University, Maritime Safety Agency, Kochi University, Tokai University, and

Geographical Survey Institute (1999), Crustal movements in Kozu Island, Izu Islands in southern Central Japan, detected by GPS measurements (July 1996 – August 1998), *Rep. coordinating committee for earthquake prediction, 62*, 241-249, 1999.

Nakamichi, H., M. Ukawa, and S. Sakai (2004), Precise hypocenter locations of midcrustal low-frequency earthquakes beneath Mt. Fuji, Japan, *Earth Planets Space, 56*, e37-40.

Nishimura, T., S. Ozawa, M. Murakami, T. Sagiya, T. Tada, M. Kaidzu, and M. Ukawa (2001), Crustal deformation caused by magma migration in the northern Izu Islands, Japan, *Geophys. Res. Lett.*, 28, 3745-3748.

Nishimura, T. (2002), Earthquake triggering due to Volcanic deformation sources in areas east off Ito and around the Mt. Iwate Volcano. (in Japanese with English abstract), *J. Geography*, *111*, 166-174.

Nishimura, T., M. Murakami, S. Ozawa, M. Ishimoto, T. Sagiya, H. Yarai, T. Tada, M. Kaidzu, and M. Ukawa (2002), Crustal deformation and source estimation before and after the 2000 Miyakejima eruption –Inflation and deflation sources from the 1983 eruption to May 2001 (in Japanese with English abstract), *Bull. Earthq. Res. Inst., Univ. Tokyo*, *77*, 55-65.

Nishimura, T., T. Hirasawa, S. Miyazaki, T. Sagiya, T. Tada, S. Miura, and K. Tanaka (2004), Temporal change of interplate coupling in northeastern Japan during 1995-2002 estimated from continuous GPS observations, *Geophys. J. Int., 157*, 901-916, doi:10.1111/j.1365-246X.2004.02159.x.

Nyst, M., T. Nishimura, F. F. Pollitz, and W. Thatcher (2006), The 1923 Kanto earthquake reevaluated using a newly augmented geodetic data set, *J. Geophys. Res.*, *111*, B11306, doi:10.1029/2005JB003628.

Ohta, Y., F. Kimata, and T. Sagiya (2004), Reexamination of the interplate coupling in the Tokai region, central Japan, based on the GPS data in 1997-2002, *Geophys. Res. Let., 31*, L24604, doi:10.1029/2004GL021404.

Okada, Y. (1985), Surface deformation due to shear and tensile faults in a half-space. *Bull. Seismol. Soc. Am. 75*, 1135-1154.

Ozawa, S., M. Murakami, M. Kaidzu, T. Tada, T. Sagiya, Y. Hatanaka, H. Yarai, and T. Nishimura (2002), Detection and monitoring of ongoing aseismic slip in the Tokai region, central Japan, *Science*, *298*, 1009-1012 (Erratum post date 18 April 2003).

Ozawa, S., S. Miyazaki, Y. Hatanaka, T. Imakiire, M. Kaidzu, and M. Murakami (2003), Characteristic silent earthquakes in the eastern part of the Boso peninsula, Central Japan, *Geophys. Res. Let.*, *30*, 1283, doi:10.1029/2002GL016665.

Pollitz, F. F. (1996), Coseismic deformation from earthquake faulting on a layered spherical earth,

Geophys. J. Int., *125*, 1-14.

Pollitz, F. F., M. Nyst, T. Nishimura, and W. Thatcher (2005), Coseismic slip distribution of the 1923 Kanto earthquake, Japan, *J. Geophys. Res., 110*, B11408, doi:10.1029/2005JB003638.

Research Group for Active Faults of Japan (1991), *Active faults in Japan: Sheet Maps and Inventories* (in Japanese), Revised ed., Univ. Tokyo Press, Tokyo.

Rothatcher, M., and L. Mervart (1996), Bernese GPS software Version 4.0, 418pp.

Sagiya, T. (1999), Interplate coupling in the Tokai district, Central Japan, deduced from continuous GPS data, *Geophys. Res. Lett.*, *26*, 2315-2318.

Sagiya, T., and W. Thatcher (1999), Coseismic slip resolution along a plate boundary megathrust: The Nankai Trough, southwest Japan, *J. Geophys. Res.*, *104*, 1111-1129.

Sagiya, T., S. Miyazaki, and T. Tada (2000), Continuous GPS array and present-day crustal deformation of Japan, *Pure Appl. Geophys.*, *157*, 2303-2322.

Sagiya, T. (2004), Interplate coupling in the Kanto district, central Japan, and the Boso Peninsula silent earthquake in May 1996, *Pure Appl. Geophys.*, 161, 2327-2342.

Satake, K., T. Baba, K. Hirata, S. Iwasaki, T. Kato, S. Koshimura, J. Takenaka, and Y. Terada (2005), Tsunami source of the 2004 off Kii Peninsula earthquakes inferred from offshore tsunami and coastal tide gauges, *Earth Planets Space*, 57, 173-178.

Sato, H., N. Hirata, K. Koketsu, D. Okaya, S. Abe, R. Kobayashi, M. Matsubara, T. Iwasaki, T. Ito, T. Ikawa, T. Kawanaka, K. Kasahara, S. Harder (2005), Earthquake Source Fault Beneath Tokyo, *Science*, 309, 462-464, doi:10.1126/science.1110489.

Savage, J. C., and R. O. Burford (1973), Geodetic determination of Relative Plate Motion in Central California, *J. Geophys. Res.*, 78, 832-845.

Savage, J. C. (1983), A dislocation model of strain accumulation and release at a subduction zone, *J. Geophys. Res.*, *88*, 4984-4996.

Sella, G. F., T. Dixon, and A. Mao (2002), REVEL: A model for recent plate velocities from space geodesy, *J. Geophys. Res., 107(B4),* doi10.1092/2000JB000033.

Seno, T., S. Stein, and A. E. Gripp (1993), A model for the motion of the Philippine Sea plate consistent with NUVEL-1 and geological data, *J. Geophys. Res., 98*, 17941–17948.

Shishikura, M. (2003), Cycle of interplate earthquake along the Sagami trough deduced from tectonic geomorphology, (in Japanese with English abstract), *Bull. Earthq. Res. Inst., Univ. Tokyo*, *78*, 245-254.

Soh, W., K. Nakayama, and T. Kimura (1998), Arc-arc collision in the Izu collision zone, central Japan, deduced from the Ashigara Basin and adjacent Tanzawa Mountains, *Island Arc, 7*, 330-341.

Stein, R. S., S. Toda, T. Parsons, and E. Grunewald (2006), A new probabilistic seismic hazard assessment for greater Tokyo, *Proc. R. Soc. A*, in press.

Stein, S. and R. G. Gordon (1984), Statistical tests of Additional plate boundaries from plate motion inversions, *Earth. Planet. Sci. Lett.*, 69, 402-412.

Stern, R., M. J. Fouch, S. L. Klemperer (2004), An Overview of the Izu-Bonin-Mariana Subduction Factory, in *Inside the Subduction Factory, Gophys. Monogr. Ser.*, vol. 138, edited by J. Eiler, pp.175-222, AGU, Washington, D. C.

Tabei, T., J. Segawa, and F. Kimata (1999), GPS observation at the Zenisu reef (in Japanese), *Chikyu Monthly*, *Extra 25*, 166-170.

Toda, S., R. S. Stein, and T. Sagiya (2002), Evidence from the AD 2000 Izu Islands swarm that stressing rate governs seismicity, *Nature, 419*, 58-61.

Toda, S., R. S. Stein, S. B. Bozkurt, and R. Nakamura (2006), A slab fragment wedged beneath Tokyo: Consequences for earthquakes, volcanism, and geography, *Nature*, submitted.

Tada, T. and M. Hashimoto (1991), Anomalous crustal deformation in the northeastern Izu peninsula and its tectonic significance –Tension Crack Model-, *J. Phys. Earth, 39*, 197-218.

Usami, T. (2003). Materials for Comprehensive List of Destructive Earthquakes in Japan, [416]-2001, University of Tokyo Press, 605 pp., (in Japanese).

Wald, D. J., and P. G. Somerville (1995), Variable-slip rupture model of the great 1923 Kanto, Japan, earthquake: Geodetic and body-waveform analysis*, Bull. Seismol. Soc. Am., 85*, 159–177.

Wallace, L. M., C. Stevens, E. Silver, R. McCaffrey, W. Loratung, S. Hasiata, R. Stanaway, R. Curley, R. Rosa, and J. Taugaloidi (2004), GPS and seismological constraints on active tectonics and arc-continent collision in Papua New Guinea: Implications for mechanics of microplate rotations in a plate boundary zone, *J. Geophys. Res., 109*, B05404, doi:10.1029/2003JB002481.

Wallace, L. M., R. McCaffrey, J. Beavan, and S. Ellis (2005), Rapid microplate rotations and backarc rifting at the transition between collision and subduction, *Geology, 33*, 857-860.

Wessel, P., and W. H. F. Smith (1998), New, improved version of the Generic Mapping Tools, *Eos Trans, AGU, 79*, 579.

Yamanaka, H. and N. Yamada (2002), Estimation of 3D S-wave velocity model of deep sedimentary layers in Kanto plain, Japan using microtremor array measurements (In Japanese with English abstract), *Butsuri-Tansa* (*J. Geophys. Exploration Jpn.*), *55*, 53-65.

Yoshioka, S., T. Yabuki, T. Sagiya, T. Tada, and M. Matsu'ura (1993), Interplate coupling and relative plate motion in the Tokai district, central Japan, deduced from geodetic data inversion

using ABIC, *Geophys. J. Int., 113*, 607-621.

Yoshioka, S., T. Yabuki, T. Sagiya, T. Tada, and M. Matsu'ura (1994), Interplate coupling in the Kanto district, central Japan, deduced from geodetic data inversion and its tectonic implication, *Tectnophysics, 229*, 181-200.

Figure Caption

Figure 1.   (a) Tectonic setting of the Japanese islands. A thick rectangle indicates the area of Figure 1b.   (b) Shaded relief map of the Kanto region and its vicinity.   Red triangles and white circles indicate active volcanoes that have erupted within the past 10,000 years, and major cities, respectively.   The Itoigawa-Shizuoka Tectonic Line (ISTL) is a geological boundary between eastern and western Japan.   The Niigata-Kobe Tectonic Zone (NKTZ) is a kinematic boundary between eastern and western Japan, deduced from geodetic data including GPS [Sagiya et al., 2000].

Figure 2. Seismicity of the study area.   Open circles denote large earthquakes (M≥6.5) shallower than 60 km since 1703.   Stars denote epicenters of three large earthquakes, the 1703 Genroku Kanto, 1923 Kanto, and 1854 Tokai earthquake source regions are shown by dashed lines. Gray dots denote microseismicity (M≥1.0) with a depth shallower than 30 km since 1998.   Thin lines represent surface traces of Quaternary faults [Research Group for Active Faults of Japan, 1991].   Bold lines indicate surface boundaries of the crustal blocks used in this study.   The location of the West Sagami Bay Fracture (WSBF) [Ishibashi, 2004] is indicated.

Figure 3.   GPS stations and leveling routes used in this study.   Squares and colored dots with route numbers indicate GPS stations and leveling benchmarks used in the inversion analysis, respectively.   Four-digit numbers give the GPS station codes whose time-series are plotted in Figure 4.   Arrows show the direction of the leveling routes whose deformation rate is plotted in Figure 6.

Figure 4. Time-series of the selected GPS sites illustrative of secular, coseismic and transient deformation recoded by the network.   Daily coordinates in ITRF 2000 are plotted.   The gray curves are fitted by least squares.   Arrows indicate major events that caused significant displacement.

Figure 5. Horizontal and vertical velocity observed at GPS (GEONET) stations during 1996-2000.   The velocity is plotted at all stations including stations not used in the inversion analysis.   Arrows are horizontal velocities in the Eurasian reference frame. Interpolated vertical velocities are plotted by colors and contour lines in ITRF2000.   The contour interval is 2 mm, and the thick contour corresponds to zero change.

Figure 6. Observed and calculated vertical velocities at leveling benchmarks. Solid circles are observed velocities relative to the first (left) benchmarks.   Open squares are calculated velocities with optimal offset to minimize the sum of difference from the observed data.   The approximate leveling direction is shown at the top of each figure.

Figure 7.   Block boundaries and rectangular fault model used in this study.   Bold gray lines indicate boundaries of the crustal blocks on surface.   Dashed rectangles indicate rectangular faults with a solid line indicating a fault upper edge.   Dots indicate volcanic point inflation (Mogi) sources. Thin broken lines west and east of Izu Peninsula represent isodepth of the subducting Philippine Sea plate proposed by Ishida (1992) and Sato et al. (2005), respectively.

Figure 8.   (a) Estimated seismic portion of fault slip rate (e.g. slip-deficit rate) resolved on each source. (b) Coupling coefficient, together with large (M≥6) earthquakes since 1703. 1703-1922 earthquakes are from Usami (2003), and Grunewald and Stein (2006) and post-1923 shocks are from JMA. Fully coupled sources are entirely seismic; a coupling of zero indicates fully aseismic behavior. (c) Data resolution of the faults and point sources. A resolution of 100% means the parameter is fully resolved by the observed geodetic data. In contrast, a resolution of 0% means the parameter is assigned purely by a priori constraint.

Figure 9.   Observed and calculated horizontal velocities at GPS stations.   Solid and open vectors represent observed and calculated velocities, respectively.   Velocity in the Central Japan Block (CJP)-fixed reference frame is plotted to facilitate the comparison. Although the map scales are different between the top and the bottom figures, the vector velocity scales are the same.

Figure 10. Residual horizontal velocity with 95% confidence ellipses.   Thin lines represent surface traces of Quaternary faults [Research Group for Active Faults of Japan, 1991].   The thick lines represent boundaries of the model blocks.

Figure 11.   Observed and calculated vertical velocities at the GPS stations.   Red and blue rectangles represent uplift and subsidence, respectively, with their sizes proportional to velocity. Solid and dotted rectangles represent observed and calculated velocities, respectively.

Figure 12.   (a) The rigid rotational part of the velocity field of the Kanto region predicted by

31

the Euler pole of the best-fit model in the Central Japan Block (CJP)-fixed reference frame.   (b) The elastic part of the velocity field predicted by the slip deficit and point sources of the best-fit model.   Broken lines with the year of the occurrence denote the source areas of M≥7.5 earthquakes. Bear in mind that the elastic deformation associated with the Pacific plate megathrust south of the 1938 swarm zone is unresolved. (c) Total velocity field predicted by the best-fit model.

Figure 13.   Relative long-term velocity on the faults of the block boundary predicted by the Euler pole of the best model.   Velocity vectors represent the motion of the footwall relative to the hanging-wall on the fault.   The PAC vectors are denoted by open vectors to distinguish the other vectors.   The IMP vectors along its eastern boundary are shifted to avoid overlapping.   The focal mechanisms of shallow (Depth <50 km) earthquakes determined by the National Research Institute of Earth Science and Disaster Prevention (NIED) from April 1996 to May 2000 [Fukuyama et al., 1998] are plotted at the epicenters determined by the Japan Meteorological Agency (JMA).

Figure 14.   Estimated location of the EUR-PHS and CJP-IMP Euler poles, with their 95% confidence ellipses.   The pole of Seno et al. (1993) is derived from slip vectors of interplate earthquakes.   The pole of Mazzotti et al. (2001) is the TOK (Tokai-south Kanto area)-IMP Euler pole, as described in their text.   A rectangle indicates the area of the inset. (Inset) Expansion of central Japan for the IMP Euler poles

Figure 15.   Observed and calculated horizontal velocities for the PHS Euler pole of Sella et al. (2003).   Solid and open vectors represent observed and calculated velocities, respectively.

Table 1. Parameters of the rectangular fault sources

Segment	Latitude (°)	Longitude (°)	Depth (km)	Length (km)	Width (km)	Strike (°)	Dip (°)	Rake (°)	Slip deficit rate (mm/yr)		Res* (%)	Long-term slip rate (mm/yr)	Hanging wall	Foot-wall
									Initial	Posterior				
A	36.8902	143.0605	10.0	158.0	110.0	204	11	269	50	68±0.9	100	76	CJP	PAC
B	37.2825	141.9444	30.0	188.0	130.0	204	23	270	10	6±1.1	100	76	CJP	PAC
C	35.7100	142.3902	10.0	176.0	105.0	192	11	272	0	0	0	62	PHS	PAC
D	35.8101	141.2401	30.0	146.0	127.0	192	23	275	0	0	0	62	PHS	PAC
E	34.2500	141.9999	10.0	100.0	100.0	180	12	260	0	0	0	59	PHS	PAC
F	34.6100	140.9000	30.0	149.0	100.0	178	30	260	0	0	0	59	PHS	PAC
G	35.2180	139.2110	3.0	24.0	30.0	290	20	307	20	18±0.4	100	27	CJP	PHS
H	35.4360	139.3880	13.3	40.0	35.0	290	20	306	20	12±0.8	100	27	CJP	PHS
I	35.0310	139.5180	3.0	37.0	30.0	308	20	326	20	28±0.5	100	27	CJP	PHS
J	35.2310	139.7090	13.3	37.0	30.0	308	20	326	20	22±0.9	100	26	CJP	PHS
K	35.4370	139.9050	23.6	43.0	33.0	308	20	324	20	5±0.9	100	26	CJP	PHS
L	34.7500	139.8000	3.0	40.0	30.0	308	20	328	20	40±0.8	100	26	CJP	PHS
M	34.9500	139.9900	13.3	40.0	30.0	308	17	327	20	27±1.0	100	26	CJP	PHS
N	35.1000	140.3800	21.0	51.0	35.0	290	5	309	20	2±0.9	100	25	CJP	PHS
O	35.4200	140.6000	24.1	51.0	35.0	285	5	302	20	18±0.9	100	25	CJP	PHS
P	34.6500	140.1700	3.0	30.0	50.0	290	16	311	30	47±0.7	50	26	CJP	PHS
Q	34.4300	140.6700	3.0	51.0	30.0	290	7	312	20	40±1.0	1	23	CJP	PHS
R	34.6822	140.7811	6.7	51.0	38.0	290	10	311	20	42±0.8	35	23	CJP	PHS
S	35.0500	140.9800	13.3	51.0	35.0	280	15	300	20	12±0.8	32	23	CJP	PHS
T	34.3600	141.8100	3.0	100.0	73.7	290	5	313	10	10±0.1	0	22	CJP	PHS
U	34.2500	138.5200	2.0	50.0	80.0	220	15	270	20	48±2.7	100	25	CJP	IMP
V	34.7180	138.5880	2.0	43.0	30.0	195	25	249	20	10±1.1	100	17	CJP	IMP
W	34.7624	138.3420	15.5	33.0	50.0	220	17	252	20	18±1.3	100	19	CJP	IMP
X	35.1000	138.6700	2.0	43.0	20.0	190	25	232	20	4±0.6	100	11	CJP	IMP
Y	35.1280	138.5000	10.5	38.0	30.0	200	25	225	20	17±0.8	100	13	CJP	IMP
Z	35.2500	138.6600	1.0	15.0	33.1	180	25	194	20	7±0.5	100	9	CJP	IMP
AA	35.3530	138.9900	1.0	32.0	33.1	250	25	220	20	4±0.4	100	5	CJP	IMP
BB	35.2190	139.1840	1.0	30.0	14.9	175	70	185	10	29±0.8	100	28	IMP	PHS
CC	34.9500	139.2130	1.0	30.5	14.9	175	70	176	10	5±1.1	100	28	IMP	PHS
DD	34.6750	139.2420	1.0	28.0	14.9	180	70	172	10	77±2.1	100	29	IMP	PHS
EE	34.4230	139.2420	1.0	50.0	14.9	210	70	191	10	59±1.9	100	28	IMP	PHS
FF	34.0330	138.9710	1.0	50.0	16.2	225	60	192	10	17±2.3	100	26	IMP	PHS

*Resolution by observed data

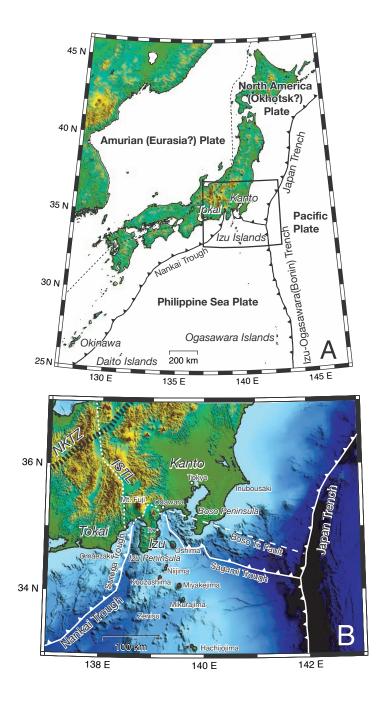Table 2. Parameters of volcanic point inflation sources

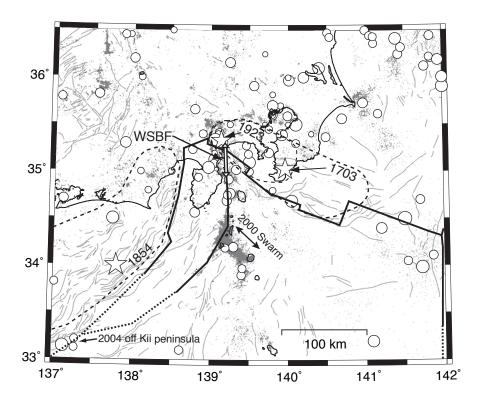| Code	Latitude (°)	Longitude (°)	Depth (km)	Volume change rate ($10^6 m^3$/yr)	Resolution by observed data (%)	Volcano Name
VA	**35.360**	**138.730**	**15.0**	3.94±0.26	99	Mt. Fuji
VB	34.969	139.152	**10.0**	3.93±0.18	100	Eastern Izu
VC	34.743	139.405	**4.0**	1.62±0.05	100	Oshima
VD	34.335	139.228	4.9	3.20±0.15	100	Niijima
VE	34.238	139.151	1.2	0.42±0.05	100	Kouzushima
VF	**34.064**	**139.513**	**9.5**	6.16±0.25	99	Miyakejima

Bold numbers represent parameters fixed values in inversion.

Table 3 Parameters of rotation Euler poles

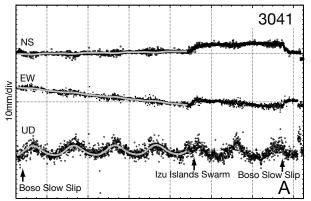| Plate	Reference plate	Latitude (°)	Longitude (°)	Rotation rate (°/m.a.)	Correlation btwn lat. and lon.
CJP	EUR	75.85±6.22	130.92±1.14	-0.351±0.045	-1.0
PAC	EUR	**63.1**	**79.2**	**-0.919**	-
IMP	EUR	36.61±0.03	138.96±0.01	-9.956±0.171	0.28
PHS	EUR	45.81±0.13	150.62±0.11	-1.592±0.016	0.79
IMP*	PHS*	34.77*	137.10*	8.410*	-

Bold numbers represent fixed parameters in the inversion. CJP: Central Japan Block, PAC: Pacific Plate, IMP: Izu Microplate, PHS: Philippine Sea Plate, EUR: Eurasia plate. *Calculated from the poles relative to EUR.
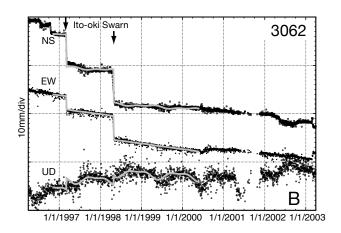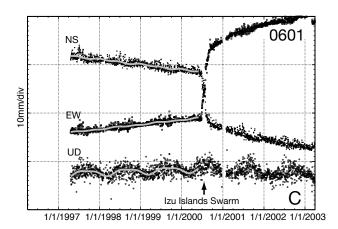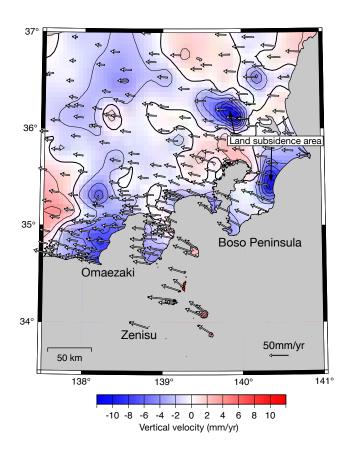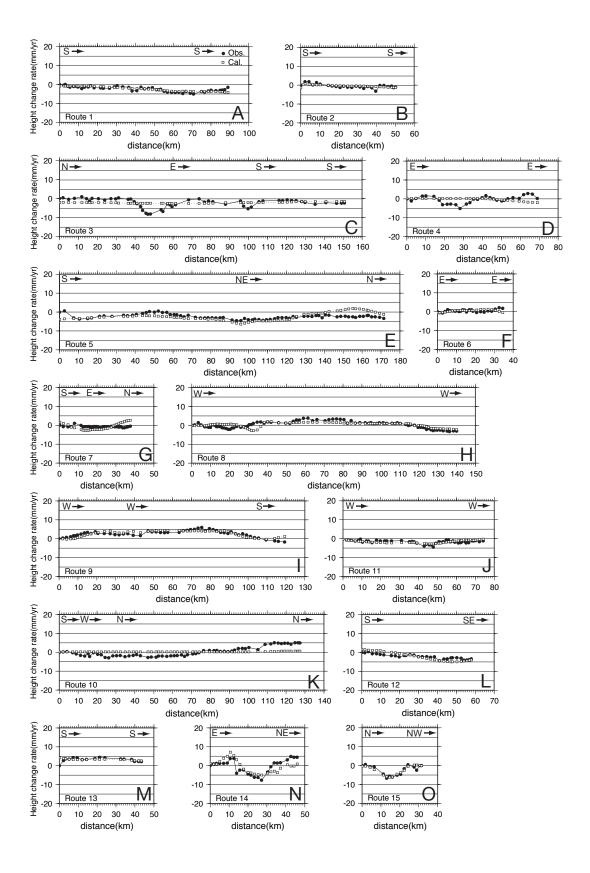
A

45 N

North America
(Okhotsk?)
Plate

40 N

Amurian (Eurasia?) Plate

Japan Trench

35 N

Kanto

Tokai

Pacific
Plate

Izu Islands

Nankai Trough

Izu-Ogasawara(Bonin) Trench

30 N

Philippine Sea Plate

Okinawa

Ogasawara Islands

25 N

Daito Islands

200 km

130 E   135 E   140 E   145 E

B

NKTZ

36 N

ISTL

Kanto

Tokyo

Mt. Fuji   Odawara

Inubousaki

Boso Peninsula

Tokai

Ito

Izu

Boso Tr. Fault

Omaezaki

Izu Peninsula

Oshima

Sagami Trough

Japan Trench

Suruga Trough

Niijima

34 N

Kouzushima   Miyakejima

Mikurajima

Nankai Trough

Zenisu

100 km

Hachijojima

138 E   140 E   142 E

Figure 1

Figure 2

Figure 3

Figure 4

Figure 5

Figure 6

Figure 7

Figure 8

Figure 9

Kouzushima

100 km

10mm/yr

Res.

Figure 10

Figure 11

A Rigid Rotation

IMP-CJP

50mm/yr   100 km

B Elastic Deformation

1938

Ashigara Mtn.

1923

1703

1854

50mm/yr   100 km

C Net Velocity

50mm/yr   100 km

Figure 12

Figure 13

Fugure 14

Figure 15